JOURNAL OF GEOPHYSICAL RESEARCH, VOL. 112, D10308, doi:10.1029/2006JD007770, 2007

Estimating daytime CO_2 fluxes over a mixed forest from tall tower mixing ratio measurements

Weiguo Wang,[1,2] Kenneth J. Davis,[1] Bruce D. Cook,[3] Chuixiang Yi,[4] Martha P. Butler,[1] Daniel M. Ricciuto,[1] and Peter S. Bakwin[5]

Received 9 July 2006; revised 19 January 2007; accepted 2 February 2007; published 23 May 2007.

[1] Difficulties in estimating terrestrial ecosystem CO_2 fluxes on regional scales have significantly limited our understanding of the global carbon cycle. This paper presents an effort to estimate daytime CO_2 fluxes over a forested region on the scale of 50 km in northern Wisconsin, USA, using the tall-tower-based mixed layer (ML) budget method. Budget calculations were conducted for 2 years under fair-weather conditions as a case study. With long-term measurements of CO_2 mixing ratio at a 447-m-tall tower, daytime regional CO_2 fluxes were estimated on the seasonal scale, longer than in earlier studies. The flux derived from the budget method was intermediate among those derived from the eddy-covariance (EC) method at three towers in the region and overall closest to that derived from EC measurements at 396 m of the tall tower. The dormant season average daytime-integrated regional CO_2 flux was about 0.35 ± 0.18 gC m^{-2}. During the growing season, the monthly averaged daytime-integrated regional CO_2 flux varied from -1.58 ± 0.19 to -4.15 ± 0.32 gC m^{-2}, suggesting that the region was a net sink of CO_2 in the daytime. We also discussed the effects on theses estimates of neglecting horizontal advection, selecting for fair-weather conditions, and using single-location measurements. Daytime regional CO_2 flux estimates from the ML budget method were comparable to those from three aggregation experiments. Differences in results from the different methods, however, suggest that more constraints are needed to estimate regional fluxes with more confidence. Despite uncertainties, our analyses indicate that it is feasible to estimate daytime regional CO_2 fluxes on long timescales using tall tower measurements.

Citation: Wang, W., K. J. Davis, B. D. Cook, C. Yi, M. P. Butler, D. M. Ricciuto, and P. S. Bakwin (2007), Estimating daytime CO_2 fluxes over a mixed forest from tall tower mixing ratio measurements, *J. Geophys. Res.*, *112*, D10308, doi:10.1029/2006JD007770.

1. Introduction

[2] Terrestrial ecosystems play a critical role in buffering the climate change caused by the carbon dioxide (CO_2) emitted from burning of fossil fuels [*IPCC*, 2001]. Quantifying the surface (ecosystem) CO_2 flux over various temporal and spatial scales can improve our understanding of the terrestrial carbon budget. Currently, it is rather difficult to measure CO_2 fluxes on regional scales [between the global and local (1 km) scales]; this has limited our understanding of the interaction between climate change and terrestrial ecosystems and resulted in significant uncertainty in predictions of future changes in climate and atmospheric CO_2 concentrations [*Schlesinger*, 1983; *Cao and Woodward*, 1998; *Huntingford et al.*, 2000; *Cramer et al.*, 2001; *IPCC*, 2001]. Direct measurements of CO_2 fluxes over a heterogeneous region are usually impractical. Therefore indirect approaches are often adopted [*Ehleringer and Field*, 1993; *Bouwman*, 1999].

[3] The convective boundary layer (CBL) budget technique is one of these indirect approaches [*Wofsy et al.*, 1988; *Raupach et al.*, 1992; *Helmig et al.*, 1998; *Levy et al.*, 1999; *Kuck et al.*, 2000; *Lloyd et al.*, 2001]. This technique itself is not new and has been applied to estimation of surface heat and water vapor fluxes based on air temperature and water vapor mixing ratio profile measurements for decades [e.g., *Betts*, 1973, 1975; *McNaughton and Spriggs*, 1986; *Betts and Ball*, 1992; *Betts*, 1994; *Gryning and Batchvarova*, 1999]. However, it is not easy to apply this technique to estimating regional CO_2 fluxes because well-calibrated CO_2 mixing ratio profiles from near the surface through the CBL are not routinely available unlike profiles of air temperature and water vapor mixing ratio. As a result, special field campaigns, for example, using aircraft or tethered balloon measurement platforms, are usually needed

[1]Department of Meteorology, The Pennsylvania State University, University Park, Pennsylvania, USA.
[2]Now at Pacific Northwest National Laboratory, Richland, Washington, USA.
[3]Department of Forest Resources, University of Minnesota, Saint Paul, Minnesota, USA.
[4]Department of Ecology, Evolutionary Biology, University of Colorado, Boulder, Colorado, USA.
[5]Climate Monitoring and Diagnostics Laboratory, National Oceanic & Atmospheric Administration, Boulder, Colorado, USA.

0148-0227/07/2006JD007770$09.00

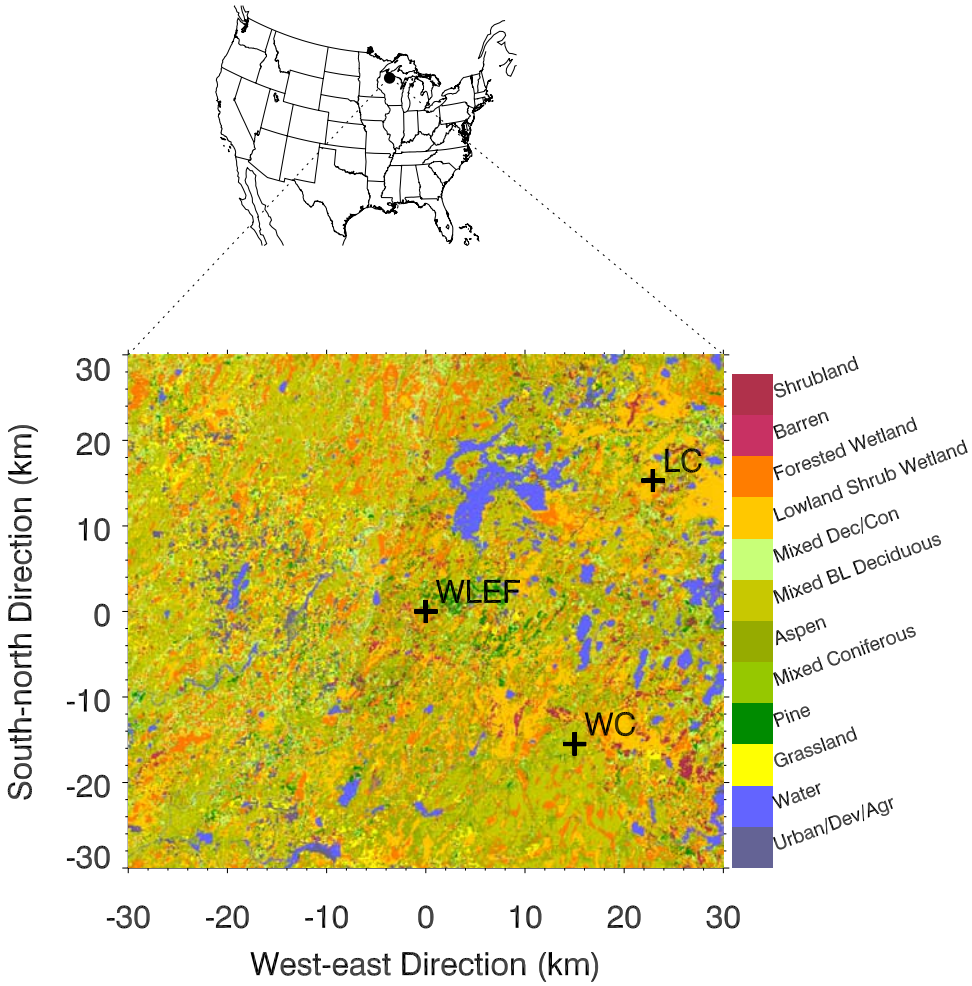

Figure 1. Location of the study site in northern Wisconsin, USA and land covers (represented by colors) in the 60 × 60-km region centered on the WLEF tower. The three pluses represent the locations of the WC, LC, and WLEF towers. Land cover data source is WISCLAND [*WiDNR*, 1998].

to conduct the budget calculation; this restricts the application of the budget technique. Additionally, field campaigns usually last only for short periods of time such as hours or days [e.g., *Kuck et al.*, 2000; *Lloyd et al.*, 2001]. Consequently, the timescales of the budget-based estimates of regional CO_2 fluxes have been on the order of days in earlier studies [*Wofsy et al.*, 1988; *Raupach et al.*, 1992; *Helmig et al.*, 1998; *Levy et al.*, 1999; *Kuck et al.*, 2000; *Lloyd et al.*, 2001]. Budget-based regional CO_2 flux estimates can be improved using the vertical profiles of CO_2 mixing ratio measured from near the surface to the midmixed-layer at a tall tower. In particular, such tall tower measurements can be made quasi-continuously for years. Therefore the timescales of regional CO_2 flux estimates based on tall tower measurements can be possibly extended beyond those in earlier studies.

[4] The main objective of this study was to explore the feasibility of applying the tall-tower-based budget method to estimating daytime regional CO_2 fluxes for long times. We used the budget method under fair-weather conditions to estimate daytime CO_2 fluxes for a region on the scale of 50 km in northern Wisconsin, USA, utilizing the continuous measurements of CO_2 mixing ratios at six levels of the 447-m-tall WLEF tower and aircraft measurements in the lower free troposphere (FT) (i.e., above the CBL). This tall-tower-based budget method provides an estimate of the daytime regional CO_2 flux that is complementary to other estimates with flux aggregation methods in the same region [*Wang et al.*, 2006a; *Desai et al.*, 2007]. This work also represents progress toward a more comprehensive application of measurements from the North American tall-tower network to quantifying regional CO_2 fluxes on longer timescales.

2. Materials and Methods

2.1. Site and Data

[5] The WLEF tall communication tower (45.9°N, 90.3°W) is located about 15 km east of Park Falls, Wisconsin, USA. The region around the tower is relatively flat with patches of wetland and uplands with mixed evergreen and deciduous forests.

[6] Fluxes of momentum, sensible heat, latent heat, and CO_2 were measured with the eddy-covariance (EC) method at the three following towers in the region: Willow Creek (WC), Lost Creek (LC), and WLEF towers (Figure 1). At WLEF, EC fluxes were measured at three levels [30, 122, and 396 m above the ground level (AGL)], and CO_2 mixing

ratio data, traceable to WMO primary standards, were collected at six levels (11, 30, 76, 122, 244, and 396 m AGL) [*Bakwin et al.*, 1998; *Davis et al.*, 2003]. Measurements at WLEF began in 1995. The land cover types in the typical daytime footprint areas for CO_2 EC flux measurements at 122 and 396 m of the WLEF tower were mainly mixed wetland and upland forests. The grassland around the tower base could contribute significantly to flux measurements at 30 m under unstable conditions [*Wang et al.*, 2004, 2006b]. The WC tower is located about 20 km southeast of the WLEF tower. EC fluxes were measured at 30 m, and CO_2 mixing ratios were measured at 0.6, 1.5, 3.0, 7.6, 13.7, 21.3, and 29.6 m AGL. The footprint area of EC flux measurements at this tower was covered mainly by upland deciduous forests. The LC tower is located in a wetland area, about 25 km northeast of the WLEF tower. EC fluxes were measured at 10.2 m, and CO_2 mixing ratios were measured at 1.2, 1.8, 3.0, 5.5, and 10.2 m AGL. Measurements at WC and LC began in 1999 and 2001, respectively. Vegetation heights ranged mostly from 2 to 25 m in the region. Similar measurement methodology and data processing techniques (including data screening criteria) are applied at the three towers [*Berger et al.*, 2001; *Davis et al.*, 2003; *Cook et al.*, 2004]. Note that net ecosystem-atmosphere exchange (NEE) of CO_2 measured with the EC technique at a tower, which is called EC NEE hereafter, is a sum of "an EC flux" and "a storage flux" below the height where the EC flux is measured. EC NEE is computed on an hourly or half-hourly basis at each tower. In this study, only daytime EC NEE data were used. The EC technique for evaluating NEE has been reviewed by *Baldocchi et al.* [1988, 2001] and *Baldocchi* [2003].

[7] Other data sets were also used to construct the CBL budget components. The mean vertical velocity was estimated from the hourly Rapid Updated Cycle (RUC) reanalysis data (with 40 km resolution) [*Benjamin et al.*, 2004] because direct reliable measurements were unavailable. The state-of-the-art RUC model assimilated observations from (but not limited to) commercial aircraft, wind profilers, rawinsondes, surface weather stations, and satellite-based data. RUC data and other reanalysis data have been successfully applied in regional CO_2 budget studies [e.g., *Bakwin et al.*, 2004; *Helliker et al.*, 2004]. The CO_2 mixing ratio in the lower FT was measured using aircraft through the NOAA/CMDL Carbon Cycle Aircraft Sampling Program [*Tans*, 1996]. Air samples were generally collected biweekly at different altitudes during a single flight using an automated Programmable Flask Package. In the case of missing aircraft data (part of 2000), FT CO_2 mixing ratios were approximated as the average of the CO_2 mixing ratios measured by NOAA in the marine boundary layer at a downstream site (AZR, 38.8°N, 27.4°W) and, in the FT, at an upstream inland aircraft profiling site (CAR, 40.9°N, 108.8°W). These CO_2 mixing ratio measurements used the same calibration standard as those at the tall tower; this rules out a systematic error in estimating the CO_2 jump across the ML.

[8] Additional CO_2 mixing ratio measurements were used to assess uncertainty or justify assumptions. CO_2 mixing ratio profiles through the CBL and into the FT were measured at this site using a powered parachute platform [*Schulz et al.*, 2004] during short field campaigns. The flights were conducted hourly from morning to afternoon on some fair-weather days in May and October 2001 and August 2002. The powered parachute data were used to assess the evolution of CO_2 mixing ratio with time both within and above the CBL. In August 2003, hourly mean CO_2 mixing ratios were also measured at 76 m above the ground on the Brule tower (46.5°N, 91.6°W) and the Fence tower (45.7°N, 88.4°W), located about 100 km northwest and southeast of the WLEF tower, respectively.

[9] For this study, we define the growing as May to September and the dormant seasons as October to April. Data from 2000 to 2003 were used for regional CO_2 flux calculations. These data were chosen because fluxes of CO_2 and water vapor were affected by a tent caterpillar outbreak in 2001 and data acquisition problems in 2002 at WLEF. The budget calculation was carried out only during the period of the CBL development (from 0800 to 1500 local standard time (LST)) during which the CBL height can be reasonably estimated.

2.2. Equations and Assumptions

[10] The theoretical framework used is a simplified CBL model in which the daytime CBL is divided vertically into the two following layers (Figure 2a): the surface layer and the well-mixed layer (ML). Therefore we will refer to the method used in this study as the ML budget method. With measurements at the tall tower, it is convenient to estimate the mean CO_2 mixing ratio within the CBL (Figure 2a), which can be written as,

$$[c]_m = \frac{1}{h}\int_0^h c\,dz = \frac{1}{h}\left\{\int_0^{h_0} c\,dz + \int_{h_0}^{h} c\,dz\right\} = \frac{1}{h}\left\{h_0[c]_{m0} + (h-h_0)[c]_{m1}\right\}, \quad (1)$$

where c is the hourly mean CO_2 mixing ratio, h is the top of the ML, h_0 is the top of the surface layer. $[c]_{m0}$ is the mean CO_2 mixing ratio within the surface layer, which was estimated from measurements at lower levels (11, 30, 76, and 122 m) of the tower; $[c]_{m1}$ is the mean CO_2 mixing ratio in the ML, which was estimated by averaging CO_2 mixing ratios measured at 244 and 396 m of the tower. As usually used in the literature [e.g., *McNaughton and Spriggs*, 1986; *Stull*, 1988; *Betts and Ball*, 1992; *Garratt*, 1992; *Raupach et al.*, 1992; *Betts*, 1994; *Denmead et al.*, 1996; *Levy et al.*, 1999; *Kuck et al.*, 2000; *Lloyd et al.*, 2001], the surface flux of CO_2, denoted by F_c, can be derived approximately from the ML budget equation of CO_2 mixing ratio, i.e.,

$$F_c \approx h\frac{\partial [c]_m}{\partial t} - \left([c]_+ - [c]_m\right)\left(\frac{\partial h}{\partial t}\right) + w_+\Delta C, \quad (2)$$

where $[c]_+$ is the mean CO_2 mixing ratio just above the ML top; w_+ is the vertical velocity at h, which was estimated by interpolating the vertical velocity from RUC reanalysis data [*Benjamin et al.*, 2004] to the level of h. The RUC vertical velocity represents the mean vertical motion of the atmosphere on the spatial scale of 40 km that was similar to the length scale appropriate to equation (2) [*Raupach et al.*, 1992; *Levy et al.*, 1999]. ΔC is the difference between $[c]_+$ and $[c]_{m1}$, which is also called the CO_2 jump. Note that CO_2

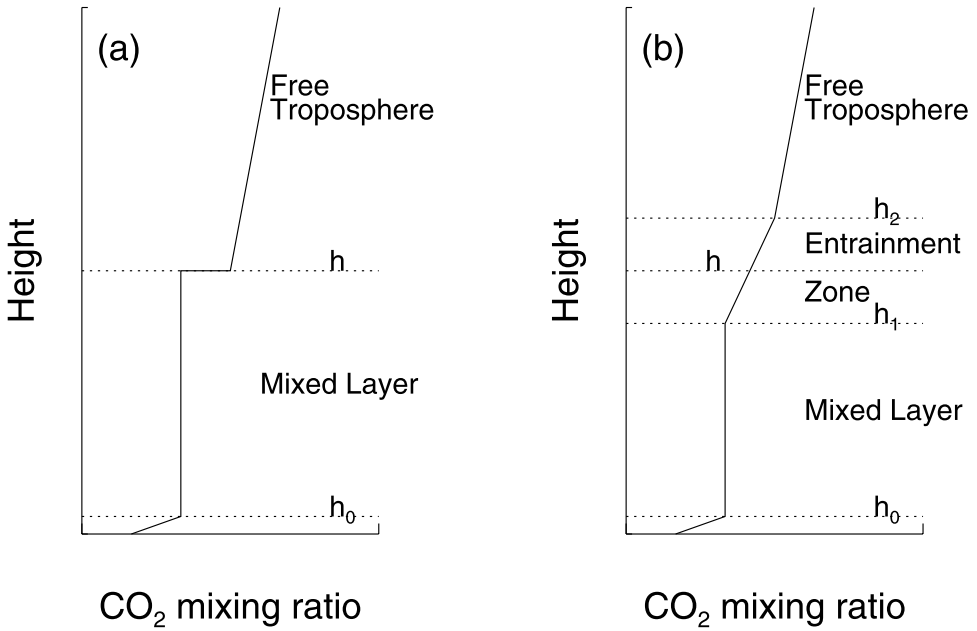

Figure 2. (a) Schematic representation of the vertical structure of the CBL in terms of CO2 mixing ratio, assuming the entrainment zone is infinitesimally thin and (b) illustrating an entrainment zone of finite thickness. h_0 is the top of the surface layer; h is the top of the mixed layer; h_1 and h_2 are the heights of the bottom and top of the entrainment zone.

mixing ratio measurements within the surface layer were included in our calculation since they were available. In this case, the CO_2 jump defined above was slightly different from $([c]_+ - [c]_m)$. Traditionally, the sum of the last two terms on the right-hand side (RHS) of equation (2) is called the entrainment flux [*Garratt*, 1992]. The first term on the RHS is called the storage flux. In deriving equation (2), three assumptions have been made in addition to the assumption that the boundary layer above the surface layer is well mixed. First, vertical advection within the surface layer was assumed to be negligible during the daytime [*Wang et al.*, 2005]. Second, the effects of horizontal advection were neglected due to lack of reliable measurements. Third, the transition layer between the ML top and FT bottom, also called the entrainment zone (EZ) (Figure 2b), was assumed to be thin compared with the ML depth, which is likely in a region under the influence of a high-pressure system with strong subsidence.

[11] Strictly speaking, equation (2) can be applied most appropriately under clear-sky conditions because the presence of fronts, deep convection, or other large-scale disturbances may make some of the assumptions for equation (2) invalid. Under fair-weather conditions, equation (2) could still present difficulties in some cases. For example, active cumulus clouds near the ML top have vigorous vertical motion and can withdraw some of the ML air into FT [*Stull*, 1988], which can neither be well represented by equation (2) nor be quantified with our data sets. Therefore these conditions should ideally be excluded in our budget calculation. Because there were not many cloud-free days at this moist forested site, fair-weather conditions with shallow clouds were included in the budget calculation in addition to the clear-sky conditions. In this case, the assumption of the negligible depth of the entrainment zone may affect the results. This is discussed in section 4.2.

2.3. Data Selection

[12] To select data for fair-weather conditions, we filtered the archived data based on incoming total shortwave (SW) radiation measurements at WC (Figure 1) (note that the incoming SW radiation was not recorded at WLEF). This approach included two steps. First, we estimated the incoming total SW radiation that can reach the measurement level (30 m) under clear-sky conditions using a simplified clear-sky radiation model [*Bird and Hulstrom*, 1991] for each hour (see the Appendix for details). Second, we took the ratio of the measured hourly incoming total SW radiation at WC to the estimated clear-sky incoming total SW radiation at the corresponding hour. The resulting ratio was called the fractional clear-sky SW radiation (FSW). If the mean FSW from 0800 to 1500 LST for a day was greater than or equal to 0.6, the day was selected and F_c was estimated using equation (2) for daytime hours. Because uncertainties in the measured radiation and the modeled clear-sky SW radiation may affect the data screening, we have reexamined the meteorological conditions for the selected days to make sure that days with precipitation, overcast, or other disturbance conditions (for example, front and deep convection) have been filtered out; this ruled out a significant error source impacting our ML-budget-based daytime CO_2 flux estimates using our data sets. In addition, the daily maximum ML height was higher than 1 km for each of the selected days, suggesting that the ML was well developed and likely to be well mixed with respect to CO_2 mixing ratio measurements. Table 1 presents the number of the selected hours (days) as well as statistical distributions of atmospheric variables during the selected hours. Approximately 25% of the selected hours were under clear-sky conditions (FSW > 0.9). During the time period from 0800 to 1500 LST, the selected days were drier than the other days in each month. The average air temperature and wind speed for the

Table 1. Distribution of Atmospheric Variables for the Selected Hours[a]

Month	Hours (Days)	FSW	PAR (μmol m^{-2} s^{-1})	w (cm/s)	Air Temperature (°C)	Wind Speed (m/s)	Relative Humidity (%)
		Median (Q1, Q3)					
March and November	98 (12)	**0.85** (0.69, 0.93)	**925** (583, 1189)	**−0.32** (−1.08, 0.42)	**−4.8** (−10, 4.9) **−3.4** (−11, 1.70)[b]	**4.2** (2.6, 4.9) **3.7** (2.7, 5.0)[b]	**57** (45, 81) **81** (63, 94)[b]
April	112 (13)	**0.84** (0.69, 0.92)	**1400** (1039, 1620)	**−1.06** (−1.90, 0.02)	**3.9** (1.9, 12.2) **5.0** (0.2, 11.2)[b]	**4.0** (2.5, 5.3) **3.8** (2.7, 5.2)[b]	**37** (26, 50) **56** (34, 87)[b]
May	229 (26)	**0.86** (0.74, 0.94)	**1564** (1281, 1784)	**0.08** (−1.73, 1.55)	**16.3** (13.7, 19.5) **14.3** (10.4, 17.9)[b]	**3.9** (3.2, 4.9) **3.7** (2.7, 4.9)[b]	**43** (34, 58) **56** (39, 81)[b]
June	202 (23)	**0.86** (0.68, 0.94)	**1524** (1246, 1725)	**−0.70** (−1.82, 0.25)	**18.4** (15.5, 20.8) **17.0** (13.2, 20.4)[b]	**3.2** (2.5, 4.0) **3.0** (2.2, 4.0)[b]	**57** (43, 71) **75** (52, 94)[b]
July	214 (28)	**0.81** (0.65, 0.92)	**1478** (1214, 1771)	**−0.65** (−1.90, 0.74)	**22.8** (19.2, 24.6) **20.7** (17.4, 23.6)[b]	**3.2** (2.2, 4.4) **3.1** (2.2, 4.1)[b]	**63** (53, 75) **73** (58, 88)[b]
August	242 (30)	**0.86** (0.77, 0.93)	**1460** (1160, 1630)	**−0.97** (−1.89, 0.05)	**22.1** (19.1, 24.0) **20.7** (17.6, 23.4)[b]	**2.9** (2.1, 4.0) **2.9** (2.1, 3.8)[b]	**66** (55, 83) **74** (60, 91)[b]
September	210 (26)	**0.86** (0.71, 0.93)	**1152** (830, 1428)	**−0.91** (−2.07, −0.04)	**14.8** (11.1, 21.0) **15.6** (10.1, 20.2)[b]	**3.1** (2.3, 4.3) **3.6** (2.6, 4.7)[b]	**60** (47, 73) **69** (53, 92)[b]
October	111 (15)	**0.80** (0.69, 0.91)	**926** (713, 1148)	**−1.21** (−2.09, −0.21)	**10.5** (5.10, 19.3) **9.0** (3.90, 14.9)[b]	**4.3** (3.1, 5.2) **3.7** (2.6, 4.6)[b]	**62** (52, 73) **72** (53, 94)[b]

[a]Each distribution is represented by the 25th (Q1), 50th (median), and 75th (Q3) percentiles of the atmospheric variable. Median values are bold. FSW = fractional clear-sky shortwave radiation reaching 30 m of the WC tower. PAR is photosynthetically active radiation. w is the mean vertical velocity in units of centimeters per second. Air temperature, wind speed, and relative humidity were measured at 30 m of the WLEF tower.
[b]The second median (Q1, Q3) in each cell shows statistical distribution of the variable during all daytime of the corresponding month (in comparison with that during the selected hours). No precipitation was recorded for the selected hours.

selected hours were not significantly different from their respective monthly averages. For all the selected hours, the median value of w_+ estimated from the RUC reanalysis product was -0.008 ms^{-1} with the 25th and 75th percentiles being -0.02 and 0.003 ms^{-1}, respectively (where positive value indicates upward motion). This suggests that the presence and growth of boundary layer clouds are limited for a majority of the selected hours. Note that the collective impacts of possible large-scale subsidence, cloud dynamics, local circulations, and other processes on the atmospheric vertical motion have been taken into account in the use of the RUC model [*Benjamin et al.*, 2004].

2.4. Estimating the ML Height, *h*

[13] Two methods were combined to estimate h because of the lack of routine direct measurements. Observational studies have suggested that the growing ML top and the lifting condensation level (LCL) may be coupled and grow together under fair-weather conditions as small cumulus begin to form over moist terrain like our forested site [e.g., *Stull*, 1988; *Betts*, 1994; *Parasnis and Morwal*, 1994]. As a result, the LCL of the ML air could be a good approximation for the ML height, particularly over moist areas [*Betts*, 1994, 2000; *Betts et al.*, 2004]. This approximation, however, may not be always true. For example, when the ML air is dry, the LCL can be very high and the ML top may not be able to reach the LCL because the ML growth is limited by other factors such as surface heating and entrainment. In this case, the ML height cannot be approximated to be the LCL height and needs to be estimated with other methods. There are many theoretical or empirical models for estimating h in the literature [e.g., *Tennekes*, 1973; *Stull*, 1988; *Garratt*, 1992; *Batchvarona and Gryning*, 1994]. In this study, we adopted an empirical model derived from radar measurements at this study site [*Yi et al.*, 2001]. The ML height was first estimated from this model and then adjusted to the LCL height if the LCL was less than the first estimate. See the Appendix for the empirical formulas for the ML [*Yi et al.*, 2001] and LCL [*Betts*, 2000] heights. Figure 3 shows the monthly diurnally averaged ML heights for the selected days in our budget calculation. In general, the ML height was lowest in August when the ML air was most moist. The

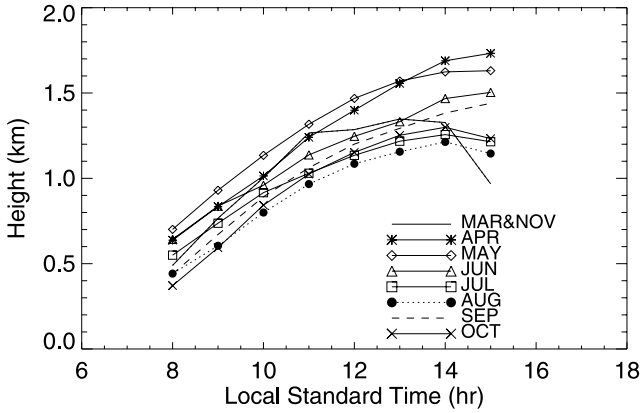

Figure 3. Estimated monthly diurnally averaged ML heights for the selected days. There are insufficient data points to calculate diurnally averaged ML heights for December, January, and February.

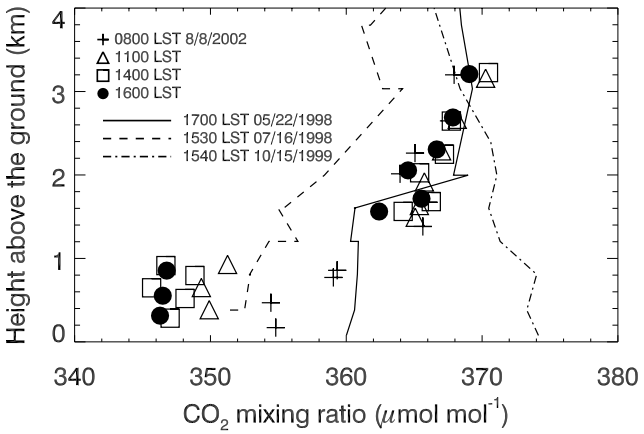

Figure 4. Examples of vertical profiles of CO_2 mixing ratio from near the surface through the lower FT measured at the WLEF site. Symbols indicate measurements from the powered parachute campaign [*Schulz et al.*, 2004], showing evolution of the profile with time for a day in summer. Lines are based on NOAA/CMDL aircraft measurements, showing typical vertical profiles of CO_2 mixing ratio in spring (solid line), summer (dashed line), and autumn (dot-dashed line). LST stands for local standard time. CO_2 mixing ratio at 3.5 to 4 km can be approximated as the baseline mixing ratio, which can be significantly different from the mixing ratio just above the ML (ML heights are about 1–1.2 km for the days shown).

ML height was highest in April and May. More discussions about the ML in the region can be found in the work of *Yi et al.* [2001]. The ML top usually reached the LCL height in the afternoon. The LCL height was used to approximate the ML height for 89% of the selected hours in the moist month of August, suggesting that the influence of small cumulus near the ML top on our budget calculation [equation (2)] might be significant. In contrast, the LCL height was used for only 34% of the selected hours in the dry winter month.

2.5. Estimating CO_2 Jump

[14] In the literature, $[c]_+$ is usually approximated to be the baseline or FT mixing ratio [*Raupach et al.*, 1992; *Denmead et al.*, 1996] or the mixing ratio measured at oceanic sites [*Levy et al.*, 1999] when direct measurements are unavailable. Such approximations, however, can result in significant errors when an air mass has passed over the continent for a long time [*Levy et al.*, 1999]. As a result, it is inappropriate to use those approximations at our continental site as shown in Figure 4 and indicated from earlier studies [*Helliker et al.*, 2004; *Yi et al.*, 2004].

[15] To a first-order approximation, we proposed a method to estimate $[c]_+$ via a combination of CO_2 mixing ratio measurements at the tall tower and aircraft profile measurements in the lower part of the FT. When the ML top was lower than 396 m, measurements at WLEF can be used as an estimate of $[c]_+$. When the ML top was higher than 396 m, $[c]_+$ was estimated with the following equation,

$$\frac{\partial [c]_+}{\partial t} \approx \left(\frac{\partial C}{\partial z}\right)_+ \left(\frac{\partial h}{\partial t} - w_+\right), \tag{3}$$

which follows a derivation by *Tennekes* [1973]. We have used the following common assumptions. First, horizontal advection above the ML was negligible compared with vertical advection. Second, the time rate of change in CO_2 mixing ratio above the ML was small compared with that within the ML, which can be justified by the observed evolution of CO_2 mixing ratio profiles within and above the ML under fair-weather conditions (powered parachute observations in Figure 4 for example). $(\partial C/\partial z)_+$ is the vertical gradient of CO_2 mixing ratio just above the ML; this vertical gradient can be nearly invariant with height in a limited layer above the ML to a certain height in the lower FT.

[16] The measured CO_2 mixing ratio profiles above the ML showed that the CO_2 mixing ratio generally decreased with height above the ML in the dormant season due to the net release of CO_2 by ecosystems, while increasing with height in the growing season due to the net uptake of CO_2 on the surface. The lines in Figure 4 show examples of CO_2 mixing ratio profiles above the ML in spring, summer, and autumn. The tropospheric profiles may not be well mixed because the exchange of CO_2 between the atmospheric boundary layer and lower FT by turbulent transport is not as efficient as mixing within the ML. Sometimes the CO2 mixing ratio above the ML can be observed to be nearly invariant with height during or shortly after synoptic disturbances such as fronts and deep convections due to large-scale mixing [*Hurwitz et al.*, 2004].

[17] To examine if the CO_2 mixing ratio can be approximated to vary linearly with height above the ML, we fitted the CO_2 mixing ratio as a linear function of height above the ML to 3500 m for each of the available vertical profiles of CO_2 mixing ratio from the powered parachute flights under fair-weather conditions. The coefficients of the determination (r^2) were calculated to assess how well the linear function can explain the variation of CO_2 mixing ratio with height above the ML. We divided the powered parachute profiles into two categories. In the first category, the CO_2 mixing ratio can be approximated to be invariant with height compared to the CO_2 jump across the ML top when the magnitude of the variation of CO_2 mixing ratio with height (i.e., the magnitude of the slope in the linear equation) was smaller than 0.2 ppm/1 km. In this case, the variation in CO_2 mixing ratio with height above the ML to 3500 m was difficult to measure accurately due to the limited precision (about 0.5 ppm) of the instruments. Twenty-one out of the total 54 observed profiles fell into this category. The rest (33) of the profiles fell into the second category where the CO_2 mixing ratio changed significantly with height above the ML, that is, the magnitude of slope was greater than 0.2 ppm/1 km. In this case, the linear function can explain more than 80% ($r^2 > 0.8$) of the variation in CO_2 mixing ratio with height for 29 of the 33 cases.

[18] On the basis of this analysis, we approximated the CO_2 mixing ratio gradient to a first order as,

$$\left(\frac{\partial C}{\partial z}\right)_+ \approx \frac{[c]_+ - C_H}{h - H}, \tag{4}$$

where H was taken as 3500 m from the data analyses in this region; C_H is the CO_2 mixing ratio at H for a given time, which was estimated by fitting the averaged NOAA/CMDL

aircraft measurements between 3 and 4 km as a function of time. The value of $[c]_+$ estimated from tall tower measurements provided the initial condition for equation (3) as the ML was developing and close to the top level of the tall tower in the morning of a given day. By solving equation (3), the CO_2 jump was estimated during the developing period of the fair-weather ML (from 0800 to 1500 LST) (Figure 5). The CO_2 jump was negative during the dormant season, implying that the CO_2 mixing ratio was smaller above than within the ML. In contrast, the jump was positive during the growing season (solid lines in Figure 5). During the dormant season, the jump did not vary significantly with month and with time of day. During the growing season, the jump varied significantly both with month (mostly due to changes in phenology) and with time of day (in response to diurnal changes in photosynthetically active radiation (PAR)). In general, the magnitude of the CO_2 jump was larger in the summer months than in the months of late spring and early autumn. The variation in the jump from morning to midafternoon was the largest in summer. CO_2 mixing ratio can be tens of parts per million larger below than above the ML in the early morning [*Yi et al.*, 2004] (not shown here) as a result of the very high concentration of respired CO_2 accumulated near the surface in summer. With PAR increasing from morning to middle afternoon, CO_2 within the ML was rapidly assimilated by photosynthetic uptake, leading to a large positive jump in the middle afternoon. In other months during the growing season, the variation in the jump from morning to afternoon was smaller mainly due to weaker assimilation and respiration rates. It should be kept in mind that likely impacts of the residual boundary layer and clouds above the ML top have not been considered in this first-order estimate. More studies are needed in the future to improve the estimates of $[c]_+$. Nevertheless, our estimates for $[c]_+$ were an improvement on those approximated as FT values in earlier studies.

2.6. Estimating Terms in Equation (2)

2.6.1. Entrainment Flux Term

[19] The entrainment flux, characterizing the net exchange of CO_2 across the ML top, can be estimated as,

$$F_e = -\left([c]_+ - [c]_m\right)\frac{\partial h}{\partial t} + w_+\Delta C, \quad (5)$$

where the first term on the RHS represents the exchanges of CO_2 due to the varying ML top, and the second term represents changes due to vertical advection. Both terms were of the same order of magnitude (Figure 5). Diurnal changes in the first term are determined by the variations both in the CO_2 jump and in h with time. Diurnal changes in the second term are correlated mainly with those in the CO_2 jump because the vertical velocity did not significantly vary diurnally compared to the CO_2 jump. In addition, the diurnal patterns of changes in the ML height and the vertical velocity (Table 1) did not vary significantly with season compared with that in the CO_2 jump. As a result, the seasonal change in the diurnal cycle of each of the two terms in equation (5) was determined primarily by that of the CO_2 jump.

[20] The monthly diurnally averaged entrainment flux (F_e) is presented in Figure 6. The magnitude of the entrainment flux from 1000 to 1500 LST during the growing season was about 50% of the surface flux in May and September and increased to 80% in summer months. In the early morning, the entrainment flux value can have an opposite sign to the surface flux due to the negative CO_2 jump (Figures 5 and 6c, 6f, and 6g). During the dormant season, the magnitude of the entrainment flux term was larger than that of the surface flux. This large percentage of the entrainment flux relative to the surface flux suggests that accurately quantifying the entrainment flux at the ML top is important in improving regional CO_2 flux estimates.

2.6.2. Storage Flux Term

[21] In general, the mean mixing ratio of CO_2 in the CBL decreased with time as the CBL grew from morning to early afternoon at this site for all months, resulting in the storage flux term being negative. We noticed that this term was only slightly more negative in the growing season, despite much stronger CO_2 uptake at the surface, than in the dormant season (Figure 6). This was because the influence of surface CO_2 fluxes on the atmospheric CO_2 mixing ratio within the CBL was modulated significantly by the dynamics of the daytime CBL [*Denning et al.*, 1999; *Gurney et al.*, 2002]. The storage flux (in the midday) was about 20% of the surface flux in June, July, and August and 50% in May and September. Overall, the storage flux term had the same sign as F_c during the growing season, but had the opposite sign and larger magnitude during the dormant season. More notably, the storage flux term had similar magnitude but an opposite sign to the entrainment flux term during the dormant season unlike during the growing season, suggesting that the estimated regional daytime CO_2 flux (which was the sum of the two terms) was subject to more significant errors.

3. Results and Discussion

3.1. Diurnal Average of Daytime Regional CO_2 Flux and Comparisons With EC Measurements at Three Levels of the WLEF Tower

[22] During the dormant season (Figures 6a, 6b, and 6h), the estimated daytime regional CO_2 flux was generally positive from 0800 to 1500 LST and smaller from late morning to early afternoon than other periods of time in the day due to photosynthetic activity of coniferous forests in the region. Compared with the dormant season, the estimated daytime CO_2 flux was significantly negative during the growing season with the largest net uptake of CO_2 being found in June and July. The magnitude of the estimated daytime regional CO_2 flux was generally larger in the midday hours than in the early morning (for example, 0800 LST) and midafternoon (for example, 1500 LST).

[23] The estimated daytime regional CO_2 flux was comparable to daytime EC NEE measured at 396 m of the WLEF tower (open circles in Figure 6). In Figure 6 as well as in Figure 7, EC NEE had been chosen for the same hours as the ML-budget-derived daytime regional CO_2 flux could be calculated. Daytime EC NEE values measured at higher levels of the tall tower were generally closer to the budget-derived daytime regional CO_2 fluxes (Figure 7). This can be explained in part from the footprint perspective. Footprint modeling suggests the fractional weights (or contributions) from the ecosystem types in the source areas for higher-

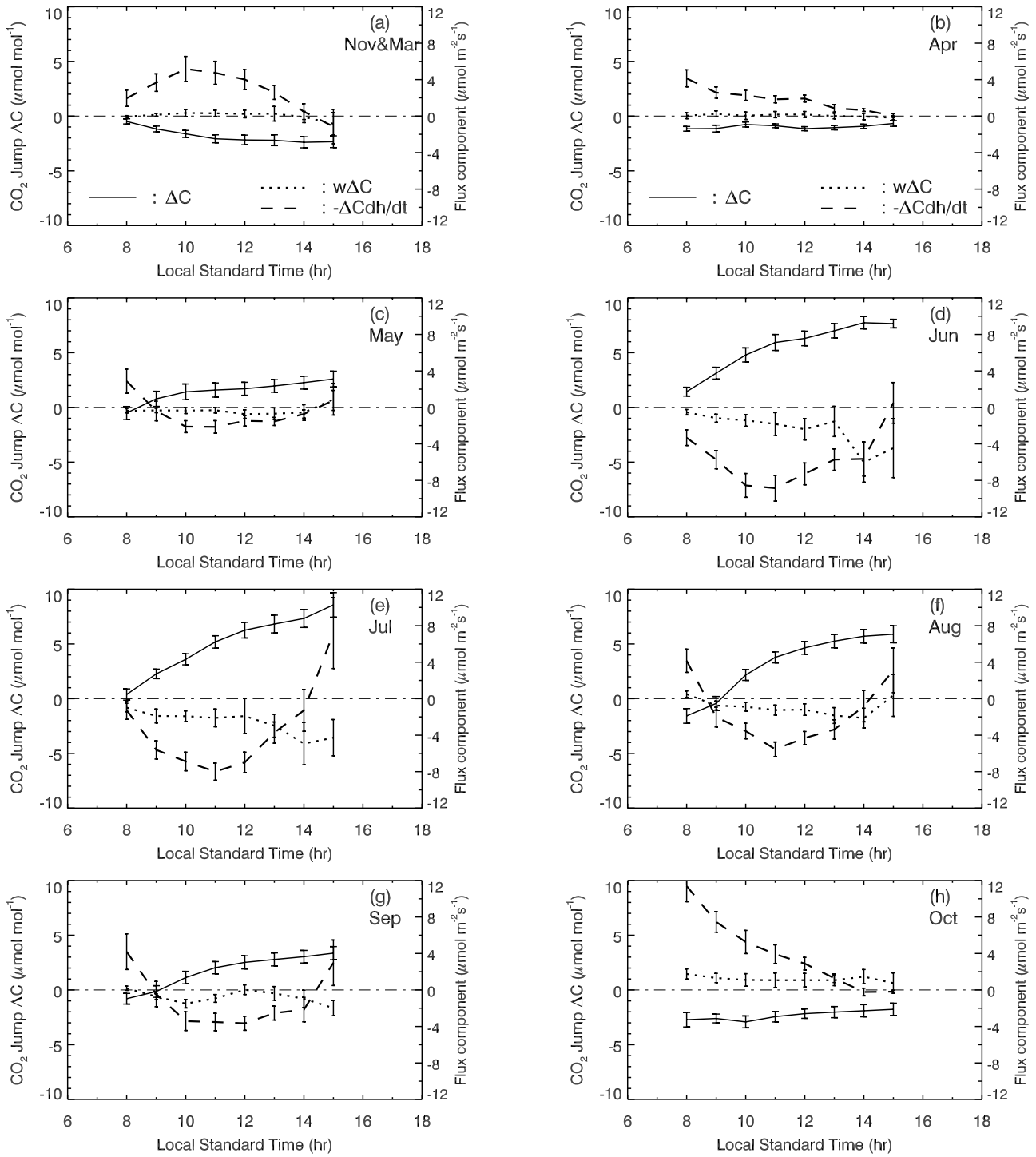

Figure 5. Diurnal average CO_2 jump ($\Delta C=[c]_+-[c]_m$), vertical advection term ($w_+\Delta C$), and entrainment flux component due to changes in ML top ($-\Delta C\partial h/\partial t$) from 0800 to 1500 LST for each month. There are insufficient data for analyses in December, January, and February. The CO_2 jump (solid line) is scaled by the left axis, while other variables are scaled by the right axis. The error bars are the standard deviations of the means.

level EC measurements were closer to the fractional areas of the respective ecosystem types in the larger 40 × 40 km^2 region [*Wang et al.*, 2004; *Wang et al.*, 2006a]. As a result, daytime EC NEE values measured at the two higher levels may approximate daytime regional CO_2 flux better than those at the lowest level, assuming that all ecosystem types in the footprint areas are representative of the entire region.

3.2. Responses of Daytime Regional CO_2 Flux to PAR and Temperature and Comparisons With EC Measurements at Three Towers

[24] We examined the responses of the estimated daytime regional CO_2 flux to PAR and to air temperature, respectively. To reduce random errors, daytime regional CO_2 flux

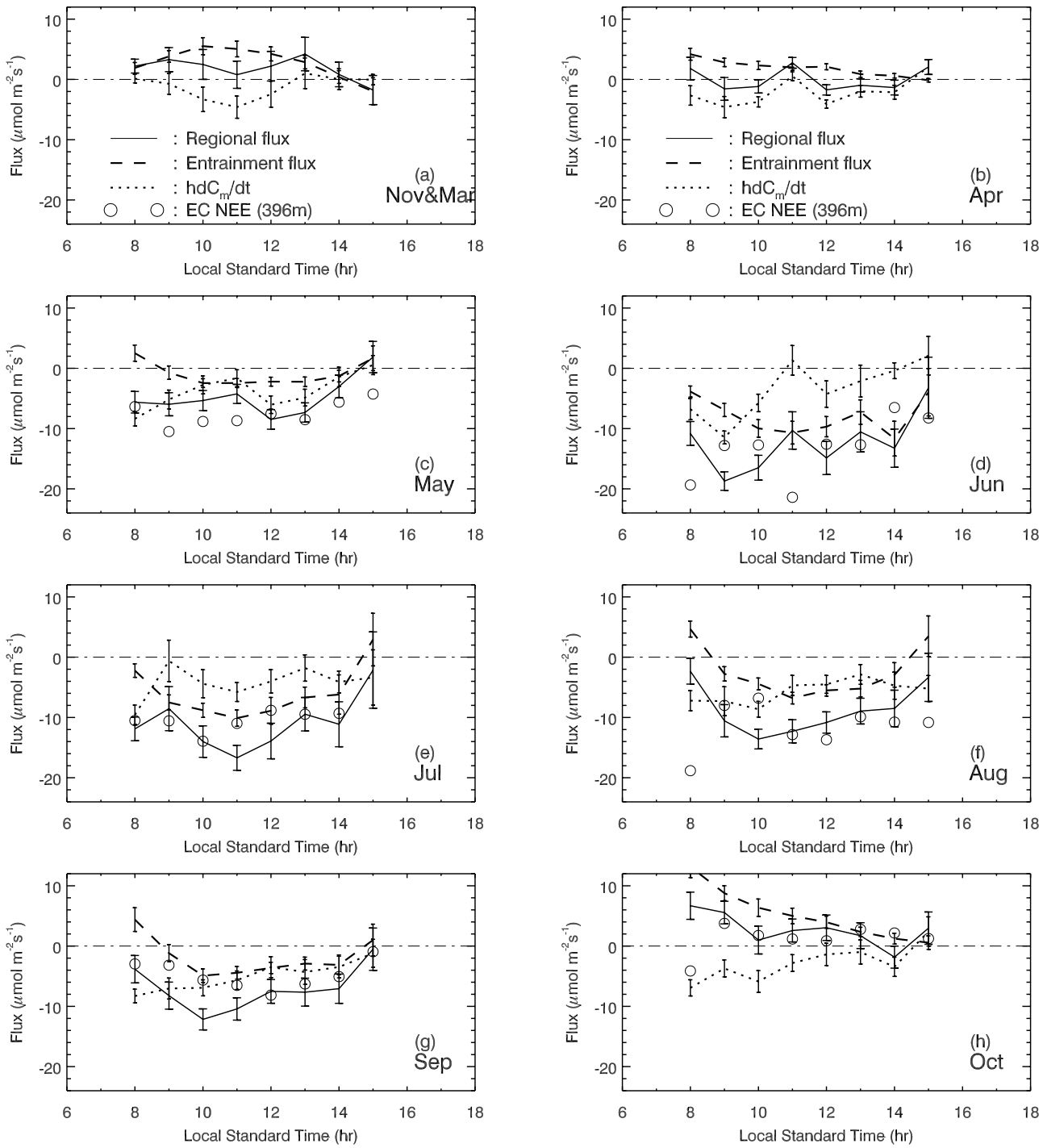

Figure 6. Diurnal averages of the calculated daytime regional flux, entrainment flux, and storage flux from 0800 to 1500 LST for each month. The diurnal average EC NEE measured at 396 m of the WLEF tower for the same hours is shown as circles for comparison. The 396-m daytime EC NEE was not available in March, April, and November when the ML-budget-derived flux was available. There are not sufficient data for analyses in December, January, and February. The error bars show the standard deviations of the means.

values were binned by PAR in increments of 200 μmol quanta m^{-2} s^{-1} starting from zero. The mean flux and its standard deviation were calculated for each bin. Figure 8 presents the bin-averaged ML-budget-derived daytime regional CO_2 flux, along with those daytime EC NEE measurements at WC, LC, and WLEF, as a function of PAR in each month. Note that all available daytime EC NEE measurements were used in the calculation. The analysis in section 4.4 suggests that differences in CO_2 flux under the selected weather conditions and under all weather conditions could be negligible for a given PAR bin during the growing season. The magnitude of daytime EC NEE

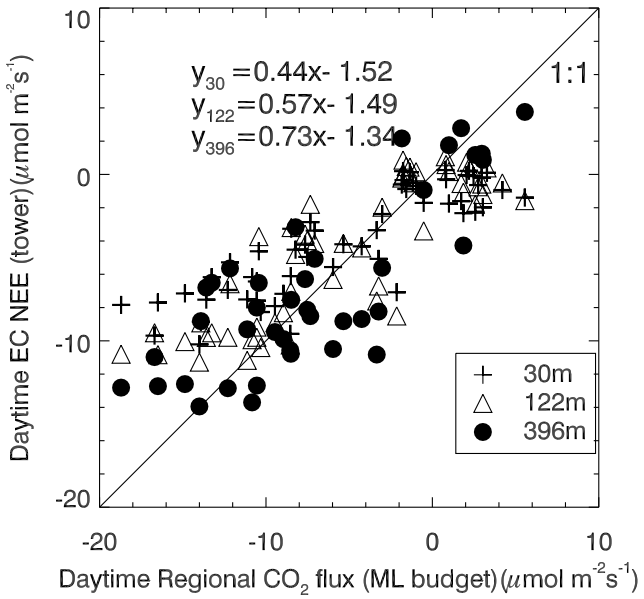

Figure 7. Comparison of the monthly diurnally averaged daytime regional flux inferred from the ML budget method (x axis) and daytime EC NEE measured at the three levels of the WLEF tower (y axis). The variables y_{30}, y_{122}, and y_{396} in the linear equations represent daytime EC NEE measured at 30, 122, and 396 m of the WLEF tower, respectively, while x represents daytime regional CO_2 flux derived from the ML budget method. Note that EC NEE values were averaged over the same hours as the ML budget calculations and EC NEE is a sum of EC flux at a height and storage flux below the height.

measured at WC was the largest for a given PAR value among all estimates during the growing season with exception of the month of May (when leaves were just starting to grow), while the magnitude of daytime EC NEE measured at LC was the smallest. Daytime regional CO_2 flux estimates were intermediate and, overall, the closest to daytime EC NEE measured at 396 m of the WLEF tower.

[25] In addition, daytime EC NEE measurements at individual stand towers showed that the ecosystem CO_2 fluxes for individual stand types tended to saturate in June, July, and August when PAR exceeded 1000 μmol quanta m^{-2} s^{-1} (Figure 8). In contrast, such saturation did not appear in the daytime regional CO_2 flux as shown in Figure 8. This was consistent with earlier findings that scaling up in time or space might ''linearize'' the light response curve and decrease the apparent quantum yield [*Ruimy et al.*, 1995].

[26] To estimate and integrate daytime regional CO_2 flux over long periods of time such as months, we tried fitting the estimated regional flux to ecosystem models that formulate CO_2 fluxes as a function of PAR or air temperature. Because the ML budget method was applied only from 0800 to 1500 LST under fair-weather conditions, the resulting flux estimates were associated with a range of large PAR values. When the ML-budget-based daytime CO_2 flux estimates were unavailable for the given PAR values, daytime EC NEE measured at 396 m of the WLEF tower was used to approximate the regional flux. This was because the 396-m daytime EC NEE was likely the closest to the regional flux among the flux tower measurements based on comparisons in previous sections. As a result, the response of the estimated daytime regional CO_2 flux to PAR can be modeled with a rectangular hyperbolic relationship [*Ruimy et al.*, 1995],

$$F_c = \frac{\alpha I P_m}{\alpha I + P_m} + R \tag{6}$$

where I is PAR (μmol quanta m^{-2} s^{-1}); P_m (μmolC m^{-2} s^{-1}) is the saturated assimilation rate; α is the apparent quantum yield (μmolC/μmol quanta), and R is the intercept that can be interpreted as the daytime respiration rate (μmolC m^{-2} s^{-1}). During the growing season, variations in the estimated daytime regional CO_2 flux with PAR can be described reasonably by the light response curve. Overall, the magnitude of the apparent quantum yield for the regional flux was smaller than when fitted from measurements at individual EC towers; this is consistent with the implication of the study by *Ruimy et al.* [1995]. The magnitude of the saturated assimilation rate (P_m) for the regional flux was intermediate among those fitted from measurements at individual EC towers, with WC having the largest value. The regional flux respiration rate (R) is also intermediate in value, with WLEF having the largest value and LC having the smallest.

[27] The response of daytime regional CO_2 flux to PAR, however, cannot be well described by the light response model (Figures 8a, 8b, and 8h) during the dormant season as a result of significantly reduced photosynthetic activities. Therefore we also examined the relationship between ecosystem CO_2 flux and air temperature. The estimated daytime CO_2 flux values were binned by the air temperature measured at 30 m of WLEF in increments of 4°C. Figure 9 shows the bin-averaged daytime regional CO_2 flux as a function of the air temperature, suggesting that daytime regional CO_2 flux estimates were generally intermediate among the daytime EC NEE values for a given air temperature during the dormant season. The response of daytime regional CO_2 flux to air temperature was modeled with an exponential equation, i.e.,

$$F_c = ae^{bT}, \tag{7}$$

where T is the air temperature at 30 m in degrees Celsius above the ground, a is SF at $T = 0$°C, and b is the coefficient describing the sensitivity of the flux to the change in temperature. The equation is identical mathematically to the widely used Q-10 model [*Lloyd and Taylor*, 1994]. Only about 30% (r^2) of the variation of the estimated daytime regional CO_2 flux with air temperature can be explained by the exponential model. Two reasons may account in part for such a low value of r^2. First, relative errors in regional flux estimates were generally larger during the dormant season than during the growing season due to the smaller magnitude of the flux as discussed in section 2.6. Second, the ML budget method aggregated the fluxes for all stand types including deciduous and coniferous forests in the region and, hence, neither the respiratory process nor the assimilation process overwhelmingly dominated in the day

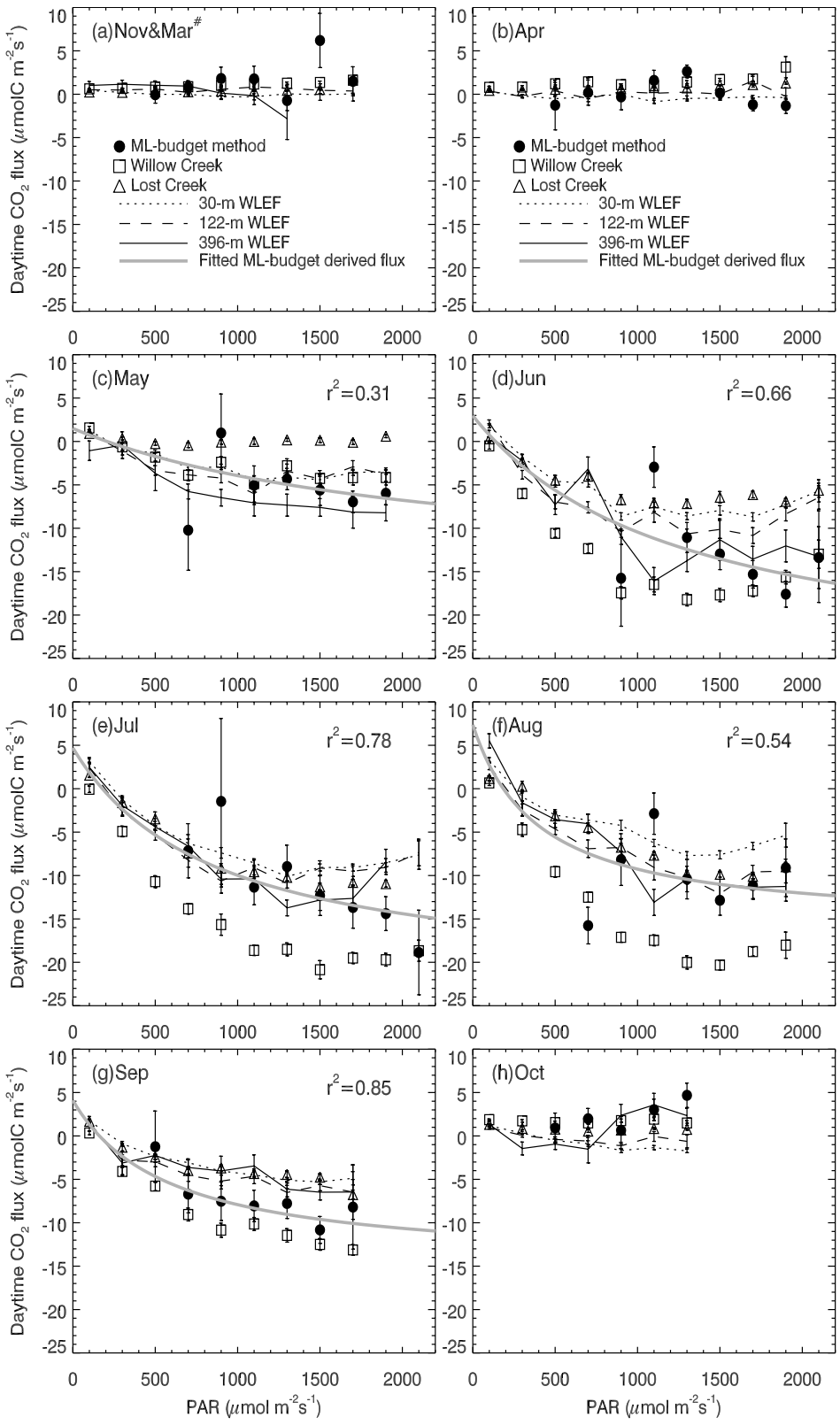

Figure 8. (a) Bin-averaged daytime CO_2 flux values inferred from the ML budget method and directly measured with the EC technique at WC, LC, and WLEF as a function of PAR in November and March, (b) April, (c) May, (d) June, (e) July, (f) August, (g) September, (h) October. There are insufficient data to show for December, January, and February. Data are binned by PAR in increments of 200 μmol quanta m^{-2} s^{-1}. The standard deviation is for the mean flux in each bin. r^2 is the coefficient of determination, indicating the degree to which the change in bin-averaged flux with PAR can be explained by the fitted curve (thick grey lines).

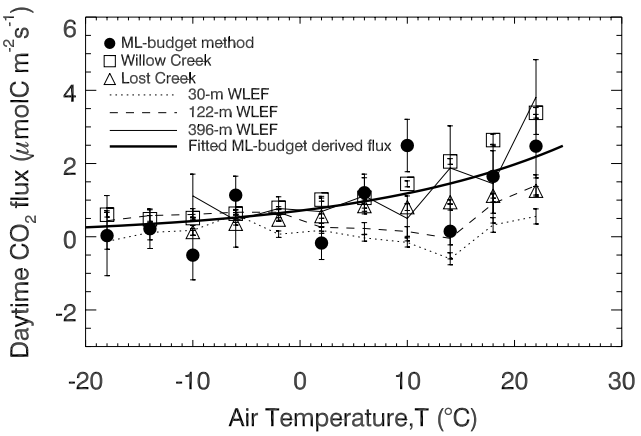

Figure 9. Bin-averaged daytime CO_2 fluxes derived from the ML budget method and directly measured with the EC technique at the three towers as a function of air temperature at 30 m (except for the LC tower where air temperature was measured at 10 m) during the dormant season from October to April. Data are binned by air temperature in increments of 4°C. Note that EC NEE data were not available in January and February and the budget-derived flux was unavailable from December through February. The error bars are the standard deviations of the means.

on the regional scale during the dormant season. This likely led to the difficulty in describing daytime regional CO_2 flux only with either the light response model or the exponential model. In other words, both temperature and PAR may be among the important factors controlling the daytime ecosystem CO_2 flux in the region. In contrast, for individual stands, temperature or PAR can be the dominant factor controlling ecosystem CO_2 flux, and therefore, changes in the flux with environmental conditions can be explained reasonably by one of the ecosystem models (equations 6 and 7).

3.3. Monthly Averaged Daytime-Integrated Regional CO_2 Flux and Comparisons With EC Measurements

[28] We hypothesized that the ecosystem models fitted to the ML-budget-derived daytime regional CO_2 flux under the selected weather conditions can represent those under all weather conditions. The possible bias is discussed in section 4.4. With this hypothesis, daytime regional CO_2 flux of each hour was calculated using equations (6) and (7) with measured PAR and air temperature at WLEF, then integrated over the daytime hours for each day. Missing hourly PAR and temperature data were approximated as their respective monthly diurnally averaged values. For comparison, the hourly EC NEE at each flux tower was also integrated over the daytime hours, where the monthly diurnally averaged EC NEE values were used for filling the missing measurements. The daytime-integrated regional CO_2 flux (DIRF) derived from the budget method was intermediate among those estimated from EC NEE measurements (Figure 10). The error bounds in the figure are the standard deviations of the mean DIRFs plus the average errors (due to model uncertainty), where we have assumed DIRFs and their errors are independent for different days, respectively. Note that possible systematic errors are not included in the error bounds. The average DIRF was estimated to be about 0.35 ± 0.18 gC m^{-2} during the dormant season, suggesting that the region was likely a small net source of CO_2 in the daytime. In the dormant season, significant differences between the DISF values and daytime EC NEE measurements were not found due to large uncertainties relative to flux magnitudes. The region was a significant net sink in the daytime during the growing season with the maximum net uptake (-4.51 ± 0.32 gC m^{-2}) occurring in June (Figure 10). ML-budget-derived daytime regional flux values are in between those derived from EC measurements at different towers or levels. DIRF values were closest to those from EC measurements at 396 m of WLEF in June, July, and August. This may not be true for other months. These comparisons and the large variability in DIRF values and EC measurements suggest that the responses of stands to similar environmental conditions over the region are significantly different, and therefore, it is not appropriate to use EC NEE measurements at any single stand tower to describe the region. Next, we will further compare ML-budget-derived DIRF to those estimated from independent methods.

3.4. Comparisons With Other Regional CO_2 Flux Estimates

[29] Regional fluxes can be estimated using different methods. Although each method may have limitations (that might result in systematic errors), it is instructive to construct a variety of regional CO_2 flux estimates. Table 2 compares the daytime regional CO_2 flux estimated from the ML budget method with those from three aggregation experiments for this region reported in the literature. In each of the aggregation experiments, the ecosystem was classified based on land cover types derived from the

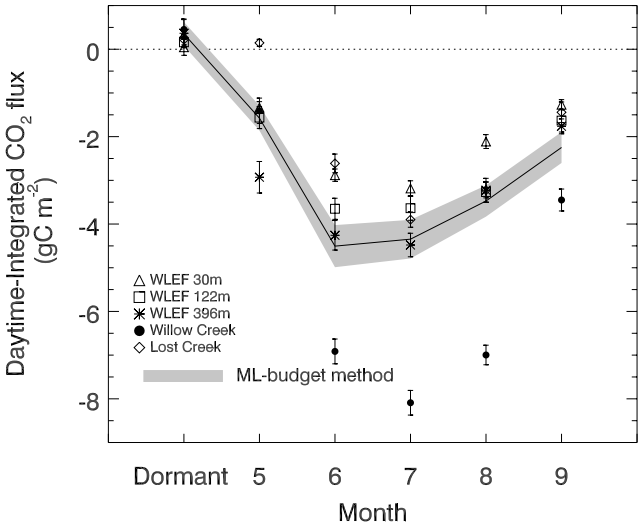

Figure 10. Comparison of monthly averaged daytime-integrated CO_2 flux derived from the ecosystem models fitted to the ML-budget-derived flux and measured with the EC technique at WC, LC, and three levels of the WLEF tower in 2000 and 2003. Data are available only in 2003 at the LC tower. 'Dormant,' data points are averaged results for months from October to April (i.e., dormant season). The error bars are the standard deviations of the means (of daytime-integrated fluxes).

Table 2. Comparison of Daytime-Integrated Regional CO_2 Flux Estimates (gCm^{-2}) From Different Methods

	Aggregation Experiments			
Methods Month	LC and WC Aggregation	Decomposition and Aggregation[a]	Multitower Aggregation[b]	ML-Budget Method
May	−0.88 ± 0.22	−2.09 ± 0.42	N/A	−1.58 ± 0.19
June	−5.44 ± 0.26	−3.90 ± 0.70	−4.17 ± 1.0	−4.51 ± 0.32
July	−6.66 ± 0.24	−4.04 ± 0.76	−5.29 ± 1.2	−4.35 ± 0.29
August	−5.71 ± 0.21	−2.91 ± 0.76	−4.42 ± 1.2	−3.47 ± 0.24
September	−2.76 ± 0.25	−1.43 ± 0.47	N/A	−2.25 ± 0.24
Dormant Season	0.37 ± 0.19	N/A	N/A	0.35 ± 0.18

[a]Aggregation experiments were conducted only during the growing season [*Wang et al.*, 2006a].
[b]Multitower aggregated scaling experiment was made using data during summer in 2003 [*Desai et al.*, 2007]. The estimated errors do not include the uncertainties due to the assumptions or simplifications used in the respective methods as well as land cover distribution errors (which might lead to systematic errors in estimated regional flux). N/A indicates that results are not available.

WISCLAND database [*WiDNR*, 1998]. Regional CO_2 flux was then estimated as the area-weighted average of the CO_2 flux values for the respective ecosystem types over a 40 × 40 km^2 region centered at WLEF. The three aggregation experiments are briefly described and discussed as follows.

[30] In the first experiment, the entire ecosystem was classified into wetland and upland on the basis of watershed functions [*Wang et al.*, 2006a]. Wetland and upland ecosystem CO_2 fluxes were assumed to be represented by the measurements at LC and at WC, respectively. Measurements in 2000 and 2003 were used. Note that measurements at LC in 2000 were unavailable and were approximated as those in 2003 in the aggregation calculation. This aggregation might overestimate the net uptake of CO_2 in summer since daytime CO_2 fluxes measured at both sites could be significantly higher in magnitude than those estimated or measured for other upland forest and wetland sites [*Wang et al.*, 2006a; *Desai et al.*, 2007]. In other words, measurements at WC and LC cannot represent all upland forests and wetlands in the region.

[31] In the second experiment, the entire ecosystem was classified into six stand types and CO_2 flux for each type was inferred by decomposing EC fluxes measured at WLEF into stand-type contribution using footprint models [*Wang et al.*, 2006a]. The inferred CO_2 flux values for the six ecosystem types were assumed to represent the entire region. Measurements in 2000 and 2003 were used. For similar land cover types, respiration rates were likely higher in the source area of flux measurements at WLEF than other areas in the region according to analyses by *Desai et al.* [2007] and *Wang et al.* [2006a]. As a result, aggregation results from this experiment might underestimate the daytime net CO_2 flux in the region.

[32] In the third experiment, the entire ecosystem was classified into 14 stand types in a similar effort to estimate regional NEE in the same region [*Desai et al.*, 2007]. Regional CO_2 flux values for each of the ecosystem types were assumed to be represented by measurements at an EC flux tower of the corresponding stand type located in an extended region across the upper midwest of USA. Measurements from June to August 2003 were used. Whether measurements at stand-level towers outside the region can represent the studied region or not was a major source of uncertainty in this experiment.

[33] In general, daytime regional CO_2 fluxes derived from the budget method were reasonably comparable to those from the aggregation experiments. A number of reasons may account for differences in the regional flux estimates. Three of them are discussed here.

[34] First, the budget-based method suffers from nonuniform time-varying source areas and land cover percentages over the areas within a heterogeneous ecosystem. Although the size of the source area is of the same order as that of the region over which the aggregation experiments were made, it is hard to accurately quantify the land cover percentages (over the source area) that may change with meteorological conditions.

[35] Second, how well the EC NEE measurements for individual ecosystem types (based on a given classification scheme) on local scales are representative of the studied region is uncertain and challenging to verify. This issue arises not only because of flux measurement errors themselves, but also because of the selection of classification schemes [*Wang et al.*, 2006a]. A widely used ecosystem scheme is based on land cover types. Ecosystem CO_2 fluxes, however, are also dependent on other ecosystem features such as soil types, stand ages, forest management, and canopy density [*Wirth et al.*, 2002; *Euskirchen et al.*, 2003; *Litvak et al.*, 2003; *Litton et al.*, 2004; *Wang et al.*, 2006a; *Desai et al.*, 2007]. More detailed classification schemes, which are not limited to land cover types, may be needed to more accurately estimate regional fluxes with aggregation methods.

[36] Finally, surface fluxes derived from the one-dimensional tower-based EC system and from the ML budget method are subject to systematic errors associated with assumptions used, which may lead to biased estimates. Uncertainties in EC NEE measurements have been discussed extensively in the literature [e.g., *Goulden et al.*, 1996; *Moncrieff et al.*, 1996; *Mahrt*, 1998]. Next, we discuss uncertainties in the ML budget calculation.

4. Uncertainties

4.1. Uncertainties due to use of Measurements at the Single Location

[37] The vertical profiles of CO_2 mixing ratio measured at a single location, which were assumed implicitly to be representative of the region, were used to calculate the storage flux term and the entrainment flux term. We

compared the time rate of change of CO_2 mixing ratio measured at 76 m of the WLEF tower, Brule tower, and Fence tower in the daytime under fair-weather conditions in August 2003. The time derivative at the WLEF site deviated from the average of those at the three towers, on average, by 0.0012 ± 0.0007 μmol m^{-3} s^{-1}, where the error bound is the standard deviation of the mean. With a typical ML height of 1000 m, the monthly average error in the storage flux due to sampling at a single location was about 1.2 μmol m^{-2} s^{-1}, assuming that the time derivative of the mean CO_2 mixing ratio in the whole CBL can be approximated by the 76-m measurement [*Yi et al.*, 2001]; this error was about 10% of the daytime CO_2 flux in magnitude.

[38] For the entrainment flux term, we can only make a crude evaluation because observational data of the horizontal gradients of CO_2 mixing ratio are unavailable. Provided that the difference of CO_2 mixing ratio was about 1 to 2 μmol mol^{-1} over a horizontal distance of 40 km in the day under fair-weather conditions during the growing season and that the horizontal gradient of CO_2 mixing ratio above the ML top was negligible compared with that within the CBL, the resulting error in the entrainment flux term would be 0.4 to 0.7 μmolC m^{-2} s^{-1} in the afternoon given that the growth rate of the ML depth was negligible and the mean vertical velocity was -0.01 ms^{-1}. This error was negligible compared to the typical daytime CO_2 flux magnitude of 15 μmol m^{-2} s^{-1} in the growing season. During the developing period of the ML, the error, however, would be larger due to the large entrainment velocity. For instance, with an increase of 200 m in the ML depth per hour occurring in the morning, the error would be about 2 to 4 μmol m^{-2} s^{-1}, which was about 10 to 20% of the daytime regional CO_2 flux estimate.

4.2. Effects of the Entrainment Zone at the top of ML

[39] The depth of the entrainment zone (EZ) at the top of ML was neglected in estimating the surface flux. Typically, the fair-weather EZ is about 20% of the mean depth of the ML as indicated by observations [e.g., *Davis et al.*, 1997]. We evaluated the changes of the storage flux and entrainment flux terms in equation (2) when a finite EZ depth was taken into account. We assumed that the EZ depth was a constant fraction (20%) of the ML depth. To facilitate calculation, the CO_2 mixing ratio was assumed to vary linearly with height within the EZ and the mean height of the ML top was in the middle of the EZ (Figure 2b). With the finite EZ, the monthly average of the storage flux term increased by approximately 10% of the magnitude of the surface flux compared with that with no EZ during the growing season. This was offset by a decrease of similar magnitude in the monthly average of the entrainment flux term. In the dormant season, there was a similar balance in the decrease of the storage flux and increase of the entrainment flux as a percentage of the magnitude of the surface flux. Even if the EZ depth was doubled, the relative change in daytime regional CO_2 flux estimates was still small despite the resulting change of each term increasing by a factor of about 1.5 to 2.

[40] For an extreme case where the bottom of EZ was located at the ML top (i.e., $h_1 = h$ in Figure 2b), a difference in daytime regional CO_2 flux with and without the EZ being considered would be about 10% if the EZ depth was assumed to be 20% of the ML depth. In other words, CO_2 uptake and release may be underestimated by 10% during both growing and dormant seasons under this extreme condition. Note that the effects of the EZ on the CO_2 jump (the difference in CO_2 mixing ratio at h_1 and h_2 in this case) had been considered in this evaluation.

4.3. Effects of Horizontal Advection

[41] Direct evaluation of the horizontal advection term in the budget equation requires high-precision measurements of horizontal distribution of CO_2 mixing ratio, which is not available without an array of instruments. Attempts have been made to estimate the effects of the horizontal advection using the spatial distribution of water vapor mixing ratio [*Wang*, 2005]. A brief summary is given here.

[42] The effects of horizontal advection on daytime regional CO_2 flux estimates due to the heterogeneous distribution of the surface vegetation at this site were preliminarily assessed on a 40-km scale in eight wind direction sectors. The overall magnitude of the effects was less than 15–20% of the flux in each wind direction in the early afternoon (from noon to 1500 LST) during the growing season. When the winds were from the northeast, east, and southeast directions, the horizontal advective fluxes ($\int_0^h U(\partial c/\partial x)\mathrm{d}z$, where U is the horizontal wind speed; x is the horizontal coordinate along with the wind direction.) were likely positive (suggesting that the surface flux is underestimated due to the neglect of the horizontal advective flux term), while they were likely negative when the winds were from the southwest, west, and northwest directions. In other wind directions, the sign of the horizontal advective fluxes could not be determined. The monthly average effects of horizontal advection on the regional flux estimates derived from the one-dimensional budget equation in this study ranged likely from -1.7 to 0.64 μmol m^{-2} s^{-1} in May, from -2.06 to 0.30 μmol m^{-2} s^{-1} in June, from -2.36 to 0.33 μmol m^{-2} s^{-1} in July, from -1.8 to 0.68 μmol m^{-2} s^{-1} in August, and from -2.5 to -0.02 μmol m^{-2} s^{-1} in September. The effects depended both on the wind direction frequency and on the horizontal advection in each wind direction. In the evaluation, the seasonal mean contribution of horizontal advection in each wind direction was used approximately for each month. The overall estimates suggest that the impact of neglecting the horizontal advection on daytime regional flux estimates may be smaller than 10–15% of the flux in magnitude during the growing season. For a more accurate evaluation, direct measurements of horizontal advection are needed eventually to eliminate the uncertainty due to the neglect of the effects of horizontal advection.

4.4. Impacts of the Selected Weather Conditions on Daytime Regional CO_2 Flux Estimates

[43] In section 3.2, we have hypothesized that the ecosystem models fitted to the ML-budget-derived daytime regional CO_2 flux under the selected fair-weather conditions can represent those under all weather conditions. In other words, the estimated flux is representative of the regional flux in all weather conditions for a given PAR during the growing season and for a given air temperature during the dormant season, respectively. Varying temperature and humidity values of soil and air under different weather

conditions can affect the net CO_2 exchange rate of ecosystem. Because of the limited number of hours when the budget calculation could be made, it was unlikely that we could isolate the dependence of the regional flux on the individual variables. Instead, we used daytime EC NEE measured at high levels of the WLEF tower to directly compare the fluxes under all weather conditions and under the selected fair-weather conditions to examine the hypothesis.

[44] For each month during the growing season, 396-m daytime EC NEE was averaged over PAR bins in an increment of 200 μmol quanta m^2 s^{-1} starting from 600 to 2000 μmol quanta m^2 s^{-1} under all weather conditions and under the selected fair-weather conditions, respectively. The average difference in the bin-averaged daytime EC NEE values for the given PAR values was about -0.1 ± 1.2 μmol m^2 s^{-1}, where the error bound was the standard deviation of the differences. During the dormant season, daytime EC NEE measured at 122 m of the WLEF tower was used because available 396-m daytime EC NEE data points were not enough under the selected fair-weather conditions. Similarly, 122-m daytime EC NEE was averaged over temperature bins in increments of 4°C starting from −20°C. The average difference was 0.4 ± 1.0 μmol m^2 s^{-1}.

[45] Provided that the above evaluations can be applied to the daytime regional CO_2 flux estimates, the daytime integrated regional flux, which was estimated from the light response model fitted to the ML-budget-based daytime regional CO_2 flux in section 3.2, is representative of all weather conditions with an relative error smaller than 10% during the growing season. The small impact of the selected weather conditions on our regional flux estimates for a given PAR was due to the strong dependence of CO_2 fluxes on PAR in the growing season. During the dormant season, the impact of weather conditions on our regional flux estimates for a given temperature could be larger since the temperature was not an overwhelmingly dominant factor controlling CO_2 fluxes in the region as discussed in section 3.2. Under weather conditions such as cloudy or overcast days, CO_2 uptake by coniferous forests and grass in the region could be significantly weaker than under fair-weather conditions for a given air temperature due to weaker PAR. In this case, net CO_2 release in the daytime would have been underestimated using the temperature-dependent ecosystem model [equation (7)] that was fitted to the estimated daytime regional flux under fair-weather conditions. On the basis of the evaluation from the tower data, the dormant season daytime-integrated regional flux (under all weather conditions) in section 3.3 could be underestimated by a factor of 20%.

4.5. Other Error Sources

[46] Uncertainties in estimating the ML depth, the vertical velocity at the ML top, as well as the CO_2 jump, could result in significant errors in CO_2 flux estimates particularly on short timescales because these quantities were used to compute the entrainment flux which contributed more than 50% of the surface flux magnitude by the calculations in this study. These errors cannot be quantified without measurements. Although assumptions were made to estimate those quantities in this study, the comparison of daytime regional CO_2 flux values estimated using the ML budget method with those measured using the EC technique at the towers indicates that the ML budget method produced reasonable patterns of the diurnal variation and magnitudes of regional fluxes on the monthly scale, which was superior to the methods that can only estimate to within an order of magnitude [*Denmead et al.*, 1999].

5. Summary and Conclusions

[47] With the long-term measurements of CO_2 mixing ratio profile at the 447-m-tall WLEF tower, monthly averaged daytime CO_2 fluxes were estimated over a region with the area of the order of 50 km using the ML budget method. The results indicate that it is feasible to apply the tall-tower-based ML budget method in estimating daytime regional CO_2 fluxes and extending the timescales of the estimates.

[48] The budget calculation was made during daytime hours (from 0800 to 1500 LST during the developing period of the ML) under the selected fair-weather conditions (mostly cloud-free or shallow cumulus conditions). A first-order model was used to estimate the CO_2 mixing ratio just above the ML top, giving reasonable diurnal and seasonal changes in the CO_2 jump across the ML top. The analyses showed the following:

[49] (1) During the growing season, the magnitude of the storage flux term was smaller than that of the entrainment flux term, while both terms were similar in magnitude with opposite signs during the dormant season. As a result, the estimated daytime regional CO_2 flux during the dormant season could have larger errors than during the growing season.

[50] (2) Net CO_2 exchange rates measured from stand-level towers tended to saturate when PAR exceeded 1000 μmol quanta m^{-2} s^{-1} during the summer. This was not the case for the estimated daytime regional flux. Daytime regional CO_2 flux estimates can be described reasonably by a light response model during the growing season. They can be described better by a temperature-dependent exponential model than by the light response model during the dormant season.

[51] (3) The region could be a net source of CO_2 in the day during the dormant season. During the growing season, the region could be a net sink of CO_2 in the day with the maximum uptake occurring in June. Among the three levels of the WLEF tower, daytime NEE observed with the EC technique at the top level was generally the closest to the fluxes derived using the budget method.

[52] (4) Daytime regional CO_2 flux estimates in this study were comparable to those inferred from three aggregation experiments reported in the literature. The differences among all the regional estimates, however, suggest that more constraints are needed to estimate regional fluxes with more confidence.

[53] (5) Uncertainties due to the use of measurements at a single location and neglecting horizontal advection might be smaller than 10–20% of the magnitude of the surface flux. Neglecting the effects of the entrainment zone at the ML top might result in an error smaller than 10%. Daytime-integrated regional flux (under all weather conditions) was likely underestimated by 20% during the dormant season (i.e., an underestimate of net CO_2 release) for it was derived from an ecosystem model fitted to the ML-budget-derived CO_2 fluxes available only under fair-weather conditions.

The impact of the selected fair-weather conditions on the fitted light response model (and hence the derived daytime-integrated regional CO_2 fluxes) was negligible during the growing season.

[54] The magnitude of the entrainment flux was more than 50% of that of the surface flux, suggesting that accurately quantifying the entrainment flux is important to improving daytime regional flux estimates. This is a major disadvantage of applying the ML budget method because it is difficult to measure the CO_2 jump and entrainment velocity around the ML top with ground-based instruments. An advantage of the ML method is that it aggregates the fluxes for all stands in the region; this can be used to constrain the estimates from open-ended bottom-up methods. However, it should be kept in mind that estimating daytime regional fluxes on short timescales (for example, hours) with the budget method is still difficult in that errors due to assumptions or approximations may be significant.

[55] In short, the vertical profiles of CO_2 mixing ratio measured at the tall tower enable a more accurate budget calculation in the ML, where the ML CO_2 mixing ratio can be directly measured. The reasonable estimates of the daytime regional CO_2 flux suggest that it is technically promising to apply the CO_2 mixing ratio profiles measured at a tall tower to inferring regional fluxes on longer timescales. More accurate evaluation could be made if measurements were expanded in the following ways: (1) The CO_2 mixing ratio just above the ML should be measured, or reliable models developed to estimate it as a function of variables should be routinely measured. (2) Approaches to estimating the mean vertical velocity at the ML top with more confidence are needed. (3) Roles of boundary layer clouds need to be quantified since those clouds often appear over moist areas. (4) Measurements of CO_2 mixing ratio within the CBL need to be made at more locations to consider the effects of horizontal heterogeneity on NEE estimates. (5) Parallel budget analyses of heat and water vapor may help quantify uncertainty in estimating ecosystem CO_2 fluxes.

Appendix A

[56] The height of the growing ML, $h(t)$, can be estimated by,

$$h(t) = a + b\sqrt{\int_0^t \left(\overline{w'\theta'}\right)_s \mathrm{d}t'},$$

where t is time; $(\overline{w'\theta'})_s$ is the surface virtual potential temperature flux; $t = 0$ is the time when $(\overline{w'\theta'})_s = 0$ in the morning; $a = 97.1$ m and $b = 25.537$ $m^{1/2}/K^{1/2}$. The model was fitted to the height of the ML top derived from the measurements of a 915-MHz boundary layer profiling radar deployed in the WLEF site in 1998 and 1999. Details were given by *Yi et al.* [2001].

[57] The LCL height, h_{LCL} (m), can be estimated approximately by

$$h_{LCL} = p(1 - \mathrm{RH})/\{A + (A - 1)\mathrm{RH}\}/\rho_a g,$$

[*Betts*, 2000; *Betts et al.*, 2004], where RH is the relative humidity at the base of the ML; p is the surface pressure (pa); $A = 0.622\lambda / (2C_pT)$; λ is the latent heat of vaporization and C_p is the specific heat of air at constant pressure; ρ_a is air density; g is the gravitational acceleration.

[58] Clear-sky incoming total shortwave radiation was estimated hourly for the WC site (45.8°N, 90.1°W) using a simplified clear-sky radiation model [*Bird and Hulstrom*, 1991]. In the calculation, ozone and water vapor thicknesses of atmosphere were taken as 0.3 and 1.5 cm, respectively. Aerosol optical depths were taken as 0.05 and 0.1 at wavelengths of 380 and 500 nm of the incoming shortwave radiation, respectively. Forward scattering of incoming radiation was 0.85. Atmospheric pressure measured at 30 m of the WC tower was used. The estimates of the clear-sky radiation were rudimentary, but still useful for screening data in this study. We have reexamined the selected days to make sure that overcast and rainy weather conditions and other conditions associated with large-scale disturbances have been excluded.

[59] **Acknowledgments.** We thank three reviewers for their insightful comments and suggestions. WLEF carbon dioxide mixing ratios, site infrastructure and maintenance are supported by the staff of the National Oceanic and Atmospheric Administration (NOAA) Earth System Research Laboratory (ESRL) Global Monitoring Division Carbon Cycle Greenhouse Gases Group (CCGG). CO_2 aircraft data were obtained from the NOAA/CMDL Carbon Cycle Aircraft Sampling Program. Model data were obtained in part from the Atmospheric Radiation Measurement (ARM) Program sponsored by the U.S. Department of Energy (DoE), Office of Science, Office of Biological and Environmental Research (BER), Environmental Sciences Division. This work was funded in part by DoE-National Institute for Global Environmental Change, DoE Office of BER Terrestrial Carbon Program, NASA Earth Science, National Science Foundation (NSF) Research Collaboration Network Grant, USDA Forest Service Global Change Research Program. Any opinions, findings, and conclusions or recommendations herein are those of the authors and do not necessarily reflect the views of DoE, NASA, NSF, and USDA. We thank John Kleist from CSU for assistance in data analyses. The authors thank Roger Strand (chief engineer for WLEF-TV) and the Wisconsin Educational Communications Board, the University of Wisconsin's Kemp Natural Resources Station, Ron Teclaw of the USDA Forest Service for additional support of this research, and numerous field crew, technicians, engineers, and students involved in installation, maintenance, troubleshooting, and data collection at all the sites.

References

Bakwin, P. S., P. P. Tans, D. F. Hurst, and C. Zhao (1998), Measurements of carbon dioxide on very tall towers: Results of the NOAA/CMDL program, *Tellus Ser. B*, *50*(5), 401–415.

Bakwin, P. S., K. J. Davis, C. Yi, S. C. Wofsy, J. W. Munger, L. Haszpra, and Z. Barcza (2004), Regional carbon dioxide fluxes from mixing ratio data, *Tellus Ser. B*, *56*(4), 301–311.

Baldocchi, D. D. (2003), Assessing the eddy covariance technique for evaluating carbon dioxide exchange rates of ecosystems: Past, present, and future, *Global Change Biol.*, *9*, 479–492.

Baldocchi, D. D., B. B. Hicks, and T. P. Meyers (1988), Measuring biosphere-atmosphere exchanges of biologically related gases with micrometeorological methods, *Ecology*, *69*, 1331–1340.

Baldocchi, D., et al. (2001), FLUXNET: A new tool to study the temporal and spatial variability of ecosystem-scale carbon dioxide, water vapor, and energy flux densities, *Bull. Am. Meteorol. Soc.*, *82*(11), 2415–2434.

Batchvarona, E., and S. E. Gryning (1994), An applied model for the height of the daytime mixed-layer and the entrainment zone, *Boundary Layer Meteorol.*, *71*, 311–323.

Benjamin, S. G., G. A. Grell, J. M. Brown, T. G. Smirnova, and R. Bleck (2004), Mesoscale weather prediction with the RUC hybrid isentropic-terrain-following coordinate model, *Mon. Weather Rev.*, *132*(2), 473–494.

Berger, B. W., K. J. Davis, C. Yi, P. S. Bakwin, and C. L. Zhao (2001), Long-term carbon dioxide fluxes from a very tall tower in a northern forest: Flux measurement methodology, *J. Atmos. Oceanic Technol.*, *18*(4), 529–542.

Betts, A. K. (1973), Non-precipitating convection and its parameterization, *Q. J. R. Meteorol. Soc.*, *99*, 178–196.
Betts, A. K. (1975), Parametric interpretation of trade-wind cumulus budget studies, *J. Atmos. Sci.*, *32*, 1934–1945.
Betts, A. K. (1994), Relation between equilibrium evaporation and the saturation pressure budget, *Boundary Layer Meteorol.*, *71*(3), 235–245.
Betts, A. K. (2000), Idealized model for equilibrium boundary layer over land, *J. Hydrometeorol.*, *1*(6), 507–523.
Betts, A. K., and J. H. Ball (1992), FIFE atmospheric boundary layer budget methods, *J. Geophys. Res.*, *97*(D17), 18,523–18,531.
Betts, A. K., B. R. Helliker, and J. A. Berry (2004), Coupling between CO2, water vapor, temperature, and radon and their fluxes in an idealized equilibrium boundary layer over land, *J. Geophys. Res.*, *109*(D18), D18103, doi:10.1029/2003JD004420.
Bird, R. E., and R. L. Hulstrom (1991), A simplified clear sky model for direct and diffuse insolation on horizontal surfaces, in *SERI Tech. Rep.*, Sol. Energy Res. Inst., Golden, CO.
Bouwman, A. F. (1999), *Approaches to Scaling of Trace Gas Fluxes in Ecosystems*, 362 pp., Elsevier, New York.
Cao, M., and F. I. Woodward (1998), Net primary and ecosystem production and carbon stocks of terrestrial ecosystems and their responses to climate change, *Global Change Biol.*, *4*(2), 185–198.
Cook, B. D., et al. (2004), Carbon exchange and venting anomalies in an upland deciduous forest in northern Wisconsin, USA, *Agric. For. Meteorol.*, *126*(3–4), 271–295.
Cramer, W., et al. (2001), Global response of terrestrial ecosystem structure and function to CO_2 and climate change: Results from six dynamic global vegetation models, *Global Change Biol.*, *7*(4), 357–373.
Davis, K. J., G. Ehret, A. Giez, J. Mann, D. H. Lenschow, S. P. Oncley, and C. Kiemle (1997), Role of entrainment in surface-atmosphere interactions over the boreal forest, *J. Geophys. Res.*, *102*(D24), 29,219–29,230.
Davis, K. J., P. S. Bakwin, C. Yi, B. W. Berger, C. Zhao, R. M. Teclaw, and J. G. Isebrands (2003), The annual cycles of CO2 and H2O exchange over a northern mixed forest as observed from a very tall tower, *Global Change Biol.*, *9*(9), 1278–1293.
Denmead, O. T., R. Leuning, M. R. Raupach, F. X. Dunin, and H. A. Cleugh (1996), Boundary layer budgets for regional estimates of scalar fluxes, *Global Change Biol.*, *2*(3), 255–264.
Denmead, O. T., R. Leuning, D. W. T. Griffith, and C. P. Meyer (1999), Some recent developments in trace gas flux measurement techniques, in *Approaches to Scaling of Trace Gas Fluxes in Ecosystems*, edited by A. F. Bouwman, pp. 67–84, Elsevier, New York.
Denning, A. S., T. Takahashi, and P. Friedlingstein (1999), Can a strong atmospheric CO_2 rectifier effect be reconciled with a 'reasonable' carbon budget?, *Tellus Ser. B*, *51B*, 249–253.
Desai, A. R., et al. (2007), Influence of Vegetation Type, Stand Age and Climate on Carbon Dioxide Fluxes Across the Upper Midwest, USA: Implications for Regional Scaling of Carbon Flux, Agric. For. Meteorol., in press.
Ehleringer, J. R., and C. B. Field (1993), *Scaling Physiological Processes: Leaf to Globe*, 388 pp., Elsevier, New York.
Euskirchen, E., J. Chen, E. G. Gustafson, and S. Ma (2003), Soil respiration at dominant patch types within a managed northern Wisconsin landscape, *Ecosystems*, *6*, 595–607.
Garratt, J. R. (1992), The atmospheric boundary layer, in *Cambridge Atmospheric and Space Science Series*, pp. xviii, 316, Cambridge Univ. Press, New York.
Goulden, M. L., J. W. Munger, S. M. Fan, B. C. Daube, and S. C. Wofsy (1996), Measurements of carbon sequestration by long-term eddy covariance: Methods and a critical evaluation of accuracy, *Global Change Biol.*, *2*(3), 169–182.
Gryning, S. E., and E. Batchvarova (1999), Regional heat flux over the NOPEX area estimated from the evolution of the mixed-layer, *Agric. For. Meteorol.*, *98–99*, 159–167.
Gurney, K. R., et al. (2002), Towards robust regional estimates of CO_2 sources and sinks using atmospheric transport models, *Nature*, *415*(6872), 626–630.
Helliker, B. R., J. A. Berry, A. K. Betts, P. S. Bakwin, K. J. Davis, A. S. Denning, J. R. Ehleringer, J. B. Miller, M. P. Butler, and D. M. Ricciuto (2004), Estimates of net CO_2 flux by application of equilibrium boundary layer concepts to CO_2 and water vapor measurements from a tall tower, *J. Geophys. Res.*, *109*(D20), D20106, doi:10.1029/2004JD004532.
Helmig, D., M. Jensen, J. Bognar, T. Smith Jr., R. Vasquez Arrieta, R. Rodriguez, J. W. Birks, B. Balsley, K. Davis, and L. R. Kuck (1998), Vertical profiling and determination of landscape fluxes of biogenic nonmethane hydrocarbons within the planetary boundary layer in the Peruvian Amazon, *J. Geophys. Res.*, *103*(D19), 25,519–25,532.
Huntingford, C., P. M. Cox, and T. M. Lenton (2000), Contrasting responses of a simple terrestrial ecosystem model to global change, *Ecol. Modell.*, *134*(1), 41–58.
Hurwitz, M. D., D. M. Ricciuto, P. S. Bakwin, K. J. Davis, W. Wang, C. Yi, and M. P. Butler (2004), Transport of carbon dioxide in the presence of storm systems over a northern Wisconsin forest, *J. Atmos. Sci.*, *61*(5), 607–618.
IPCC (2001), *Climate Change 2001: The Scientific Basis Contribution of Working Group I to the Third Assessment Report of the Intergovernmental Panel on Climate Change*, 881 pp., Cambridge Univ. Press, New York.
Kuck, L. R., et al. (2000), Measurements of landscape-scale fluxes of carbon dioxide in the Peruvian Amazon by vertical profiling through the atmospheric boundary layer, *J. Geophys. Res.*, *105*(17), 22,137–22,146.
Levy, P. E., M. Molder, P. G. Jarvis, B. Kruijt, J. B. Moncrieff, A. Grelle, and A. Lindroth (1999), Regional-scale CO_2 fluxes over central Sweden by a boundary layer budget method, *Agric. For. Meteorol.*, *98–99*, 169–180.
Litton, C. M., M. G. Ryan, and D. H. Knight (2004), Effects of tree density and stand age on carbon allocation patterns in postfire lodgepole pine, *Ecol. Appl.*, *14*(2), 460–475.
Litvak, M., S. Miller, S. C. Wofsy, and M. Goulden (2003), Effect of stand age on whole ecosystem CO_2 exchange in the Canadian boreal forest, *J. Geophys. Res.*, *108*(D3), 8225, doi:10.1029/2001JD000854.
Lloyd, J., and J. A. Taylor (1994), On the temperature dependence of soil respiration, *Functional Ecol.*, *8*(3), 315–323.
Lloyd, J., et al. (2001), Vertical profiles, boundary layer budgets, and regional flux estimates for CO_2 and its 13C/12C ratio and for water vapor above a forest/bog mosaic in central Siberia, *Global Biogeochem. Cycles*, *15*(2), 267–284.
Mahrt, L. (1998), Flux sampling errors for aircraft and towers, *J. Atmos. Oceanic Technol.*, *15*(2), 416–429.
McNaughton, K. G., and T. W. Spriggs (1986), A mixed-layer model for regional evaporation, *Boundary Layer Meteorol.*, *34*(3), 243–262.
Moncrieff, J. B., Y. Malhi, and R. Leuning (1996), The propagation of errors in long-term measurements of land-atmosphere fluxes of carbon and water, *Global Change Biol.*, *2*(3), 231–240.
Parasnis, S. S., and S. B. Morwal (1994), A convectively-driven boundary layer in the monsoon trough, *Boundary Layer Meteorol.*, *71*(1–2), 197–204.
Raupach, M. R., O. T. Denmead, and F. X. Dunin (1992), Challenges in linking atmospheric CO_2 concentrations to fluxes at local and regional scales, *Aust. J. Bot.*, *40*(4–5), 697–716.
Ruimy, A., P. G. Jarvis, D. D. Baldocchi, and B. Saugier (1995), CO2 fluxes over plant canopies and solar radiation: A review, *Adv. Ecol. Res.*, *26*, 1–68.
Schlesinger, M. E. (1983), A review of climate models and their simulation of CO_2-induced warming, *Int. J. Environ. Stud.*, *20*(2), 103–114.
Schulz, K., J. W. Birks, M. L. Jensen, B. B. Balsley, and K. Davis (2004), Tedlar bag sampling technique for vertical profiling of carbon dioxide through the atmospheric boundary layer with high precision and accuracy, *Environ. Sci. Technol.*, *38*(13), 3683–3688.
Stull, R. B. (1988), *An Introduction to Boundary Layer Meteorology*, 666 pp., Springer, New York.
Tans, P. P. (1996), Carbon cycle (Group Report), in *Summary Rep. 1994–1995*, edited by D. J. Hoffman, J. T. Peterson, and R. M. Rosson, Climate Monitoring and Diagnostics Laboratory, US Department of Commerce, Boulder, Colorado.
Tennekes, H. (1973), A model for the dynamics of the inversion above a convective boundary layer, *J. Atmos. Sci.*, *30*(4), 558–567.
Wang, W. (2005), Regional estimates of net ecosystem-atmosphere exchange of carbon dioxide over a heterogeneous ecosystem, Ph.D. thesis, The Pennsylvania State Univ., University Park.
Wang, W., K. J. Davis, D. M. Ricciuto, and M. P. Butler (2004), Footprint modeling for flux measurmenets at multiple levels from a very tall tower over a mixed forest, in *16th Symposium on Boundary Layer and Turbulence*, American Meteorological Society, Portland, ME.
Wang, W., K. Davis, B. D. Cook, C. Yi, P. S. Bakwin, M. P. Butler, and D. M. Ricciuto (2005), Surface layer CO_2 budget and advective contributions to measurements of net ecosystem-atmosphere exchange of CO_2, *Agric. For. Meteorol.*, *135*, 202–214.
Wang, W., K. Davis, B. Cook, M. Butler, and D. Ricciuto (2006a), Decomposing CO_2 fluxes measured over a mixed ecosystem at a tall tower and extending to a region using footprint models and a vegetation map—A case study, *J. Geophys. Res.*, *111*(G2), G02005, doi:10.1029/2005jg000093.
Wang, W., K. J. Davis, D. M. Ricciuto, and M. P. Butler (2006b), An approximate footprint model for flux measurements in the convective boundary layer, *J. Atmos. Oceanic Technol.*, *23*(10), 1384–1394.
WiDNR (1998), WISCLAND Land Cover (WLCGW930), Wisconsin Department of Natural Resources (WiDNR), Madison, Wisconsin.

Wirth, C., G. Hardes, M. Siry, B. Schulze, N. N. Vygodskaya, E. D. Schulze, V. Kusznetova, and I. Milyukova (2002), Comparing the influence of site quality, stand age, fire and climate on aboveground tree production in Siberian Scots pine forests, *Tree Physiol.*, *22*(8), 537–552.

Wofsy, S. C., R. C. Harris, and R. C. Kaplan (1988), Carbon dioxide in the atmospheric over the Amazon basin, *J. Geophys. Res.*, *93*, 1377–1387.

Yi, C., K. J. Davis, B. W. Berger, and P. S. Bakwin (2001), Long-term observations of the dynamics of the continental planetary boundary layer, *J. Atmos. Sci.*, *58*(10), 1288–1299.

Yi, C., K. J. Davis, P. S. Bakwin, A. S. Denning, N. Zhang, A. Desai, J. C. Lin, and C. Gerbig (2004), Observed covariance between ecosystem carbon exchange and atmospheric boundary layer dynamics at a site in northern Wisconsin, *J. Geophys. Res.*, *109*(D8), D08302, doi:10.1029/2003JD004164.

P. S. Bakwin, Climate Monitoring and Diagnostics Laboratory, National Oceanic & Atmospheric Administration, R/CMDL1, 325 Broadway, Boulder, CO 80305, USA.

M. P. Butler, K. J. Davis, and D. M. Ricciuto, Department of Meteorology, The Pennsylvania State University, 503 Walker Building, University Park, PA 16802, USA.

B. D. Cook, Department of Forest Resources, University of Minnesota, 1530 North Cleveland Avenue, Saint Paul, MN 55108, USA.

W. Wang, Pacific Northwest National Laboratory, P.O. BOX 999, K9-30, Richland, WA 99352, USA. (wang@met.psu.edu)

C. Yi, Department of Ecology, Evolutionary Biology, University of Colorado, Boulder, CO 80309, USA.